Nonlinear Circuit Design Using the Modified Harmonic Balance Algorithm

ROWAN GILMORE, MEMBER, IEEE

Abstract—**A modification to a harmonic balance algorithm allows the nonlinear analysis of circuits driven by two nonharmonically related input frequencies. The algorithm was implemented on an IBM AT Personal Computer.**

Three examples are presented to illustrate the analysis. The first is a novel wide-band FET frequency doubler that achieves an average conversion loss of 3.5 dB over the 8–16-GHz output band. The second example illustrates a technique used in the design of a *C*-band power amplifier in which third-order intermodulation distortion was reduced by 8 dB with two tones of 34 dBm each at the output. The final example illustrates the gain suppression of a smaller tone in the presence of a larger one of slightly different frequency in a limiting amplifier. Simulations agree with measurements in which 2.5-dB gain suppression was observed in a 2-GHz FET feedback amplifier driven into saturation.

I. Introduction

SOLID-STATE microwave components are all nonlinear to some degree. In communication amplifiers, any nonlinearity in the phase and amplitude of the voltage-transfer characteristics must be minimized to preserve the shape and spectral content of the signal. However, components such as limiting amplifiers, oscillators, doublers, and mixers rely on device nonlinearity for proper operation. In all cases, complete circuit analysis of these components requires a nonlinear device model and analytic means to extract the effect of device–circuit interactions from the model. This paper describes a tool to achieve this.

Characterization of a nonlinear device by a time-domain model is usually appropriate because circuit models typically relate output parameters to input parameters in a causal fashion (often through the device physics). However, a description of the linear circuit is most convenient in the frequency domain. A frequency-domain description of linear circuits is particularly advantageous at microwave frequencies as transmission lines are simply and accurately represented by phasor rotation in the complex plane, and elements such as large-bias capacitors simply map a phasor into a different magnitude and angle and pose little computational burden. A description of elements such as these in the time domain is not only difficult but would necessitate very long integration times to reach steady state. Finally, additional nodes and branches added to an existing N-port circuit do not change the size of the N by N matrix needed to represent the circuit in the frequency domain, whereas each addition represents an extra state-space equation that must be solved in the time-domain description of the circuit.

A method which weds frequency-domain linear circuit analysis to an arbitrary nonlinear device model represented in the time domain is the harmonic balance technique [1]. The purpose of this paper is to review and modify the harmonic balance procedure to allow the study of nonharmonically related inputs. Three examples will be presented. The first example is a 8–16-GHz wide-band frequency-doubler in which conversion gains of -1 to -6 dB were achieved over the octave bandwidth. The second example is a linear amplifier in which the analytical technique demonstrated a way to reduce intermodulation distortion. A 6-W amplifier was built in which the third-order intermodulation distortion products were 18 dB below two signals of $+34$ dBm each at the output. This was an 8-dB improvement over a similar amplifier without the linearization technique. The final example illustrates gain suppression in limiting amplifiers, that is, the suppression of a smaller signal in the presence of a larger signal of different frequency at the output of an amplifier driven into saturation. In all three examples, computer simulations are used to design the nonlinear circuit and to predict device behavior as a function of drive level. The results of supporting measurements are also presented.

II. The Standard Harmonic Balance Technique

The standard harmonic balance technique has been reported in many previous papers [1]–[3]. It forms the core of the analysis described, and is of such importance to microwave nonlinear circuit analysis that the technique will be briefly reviewed.

The harmonic balance technique is an iterative technique which seeks to match the frequency components (harmonics) of current in a set of branches joining two subcircuits. Duality also applies to the technique; i.e., it can match the voltage on either side of a set of nodes. For simplicity in description, only the former case will be considered here. The branches are chosen in such a way that nonlinear elements are partitioned into one subcircuit and linear elements into the other. The N branches at the linear–nonlinear interface connect the two circuits and define corresponding nodes; current flowing out of one circuit must equal that flowing into the other. Matching the frequency components in each branch satisfies the

Manuscript received March 22, 1986; revised June 26, 1986.

The author is with Schlumberger Well Services, P.O. Box 2175, Houston, TX 77252.

IEEE Log Number 8610559.

0018-9480/86/1200-1294$01.00 ©1986 IEEE

continuity equation for current. The current at each branch is obtained by a process of iteration so that dependencies are satisfied for both the linear and nonlinear sides of the circuit.

The nonlinear circuit is generally represented by a nonlinear set of equations

$$i_J(t) = g(v_1(t), \cdots, v_N(t)) \tag{1}$$

where g is an arbitrary nonlinear function (and can include differentiation and integration), and i_J and v_J are the Jth branch current and voltage, respectively. The dependent variables i_J are nonlinear functions of the independent variables v_J at some point in time T_s. Periodic, steady-state operation is assumed so that integrals and derivatives at T_s may be determined.

The linear circuit may be represented by an N by $(N+M)$ matrix, obtained by standard linear circuit analysis programs such as SUPERCOMPACT [4]. The M additional variables are the additional external nodes (or branches) at which applied voltages (or currents) are present. The linear circuit matrix is calculated at each frequency component present in the circuit. In the case of an applied input signal which contains harmonically related components at $\omega, 2\omega, \cdots, q\omega$, there will be $(q+1)$ matrices relating the independent variables at each branch to the dependent variables

$$\begin{pmatrix} v_1(k\omega) \\ \vdots \\ v_N(k\omega) \end{pmatrix} = \begin{pmatrix} H_{11}(k\omega) & H_{12}(k\omega) & \cdots & H_{1(N+M)}(k\omega) \\ H_{21}(k\omega) & H_{22}(k\omega) & \cdots & H_{2(N+M)}(k\omega) \\ \vdots & \vdots & \ddots & \vdots \\ H_{N1}(k\omega) & H_{N2}(k\omega) & \cdots & H_{N(N+M)}(k\omega) \end{pmatrix} \begin{pmatrix} i_1(k\omega) \\ \vdots \\ i_N(k\omega) \\ v_{N+1}(k\omega) \\ \vdots \\ v_{N+M}(k\omega) \end{pmatrix} \tag{2}$$

for

$$k = 0, 1, \cdots, q$$

where the $H_{ij}(k\omega)$ are impedance or transfer ratios, depending on which of the variables are voltages and which are currents. The purpose of the harmonic balance program is to find a simultaneous solution to (1) and (2) for $v_1, v_2, \cdots, v_N$ so that $i_1, i_2, \cdots, i_N$ may be determined.

Fig. 1 illustrates the application of the technique to a three-terminal device such as an FET. Two branches constitute the FET gate input and the FET drain output; these separate the nonlinear FET elements into one subcircuit and the parasitics, matching, and output networks into another (linear) subcircuit. The third branch is the source of the FET and is chosen as the reference, so that $N = 2$. Here, v_1 and v_2 are the independent variables, and i_1 and i_2 are the dependent variables. Additional applied inputs are the external voltages V_1 and V_2. The desired output variables such as the current and voltage in the load can be found once i_1 and i_2 are determined.

Equation (1) is stated in the time domain, and (2) is stated in the frequency domain. Time-to-frequency conversion is achieved using the discrete Fourier transform (DFT). If estimates of $v_J(t)$ for $J = 1, \cdots, N$ at some time T_s are substituted into (1), i_J can be found at time T_s. If this is done at time instants $T_s, 2T_s, \cdots, LT_s$, an L-point sequence of time samples of i_J results. The Nyquist sampling theorem states that if a sequence of points is obtained by a sampling a waveform at a rate that is at least twice the highest component contained, the original waveform can be reconstructed. If the waveform contains only discrete frequencies which are spaced by integral multiples of ω, up to $q\omega$, one can set

$$T_s = \frac{2\pi}{(2q+1)\omega}$$

with $L = (2q+1)$ to satisfy the Nyquist criterion, and can extract the desired frequency components at ω from the L-point sequence by using the DFT.

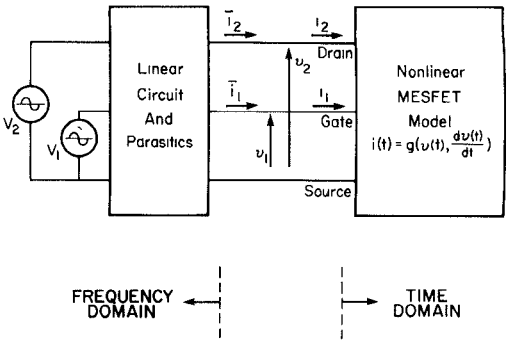

Fig. 1. Analysis of an FET by the harmonic balance method showing the partitioning of the circuit into linear and nonlinear subcircuits and the definition of the variables at the linear–nonlinear interface.

An initial estimate must be made for i_J and v_J because they are not known *a priori*. Iteration between (1) and (2) is performed using the DFT to obtain the frequency components from the time samples obtained from (1) until a self-consistent set of variables (i.e., those which satisfy the current continuity equations) is attained. The algorithm used in the analysis is as follows.

1) Initial guesses are established for the current phasors $\bar{i}_J(k\omega)$ at the interface branches at the dc, fundamental, and harmonic frequencies $(k = 0, 1, \cdots, q)$. The overbar refers to the current flowing in the linear "side" of the interface branches.

2) The hybrid matrix for the linear circuit $H(k\omega)$ is calculated at dc, the driving frequency ω, and each harmonic. This is used with $\bar{i}_J(k\omega)$ and the applied exter-

nal voltages in (2) to calculate the unknown phasor components of voltage at each of the N branches.

3) Using an expression

$$v_J(t) = \text{Real} \sum_{k=0}^{q} v_J(k\omega) e^{jk\omega t}$$

to derive the time value of the branch voltages at times $t = T_s, 2T_s, \cdots, LT_s$ and a similar expression for derivatives, the time samples of voltage and its derivatives may be calculated at each of the N branches.

4) Values of $i_J(t)$ in the nonlinear "side" of the interface branches may be obtained at corresponding time instants by substitution of the time samples of voltage $v_J(t)$ and its derivatives into (1).

5) Using the DFT, the harmonic phasor components $i_J(k\omega)$ may be extracted from the L-point sequence of $i_J(t)$ because the sequence consists of samples obtained at the Nyquist rate.

6) An error function is formed to compare the "nonlinear" current estimates i_J with the "linear" estimates $\overline{i_J}$

$$E\left(i_1, i_2, \cdots, i_N, \overline{i_1}, \overline{i_2}, \cdots, \overline{i_N}\right)$$
$$= \sum_{k=0}^{q} \left(|i_1(k\omega) - \overline{i_1}(k\omega)|^2 + \cdots + |i_N(k\omega) - \overline{i_N}(k\omega)|^2\right).$$

7) The continuity equation for current states that the "nonlinear" currents must equal the "linear" currents. This corresponds to zero error function as a solution. The error function is minimized by forming new initial guesses for the current phasors $\bar{i}_J(k\omega)$ from the old estimates, and repeating steps 2) through 7) until the error function lies below some threshold. At this point, the linear and nonlinear partitions give self-consistent results, since the currents on each "side" of the interface branches are equal. In this way, i_J and v_J are determined, and the voltage (or current) can be found at any desired node in the circuit (e.g., at the load) by linear analysis.

The fixed-point method of Hicks and Khan [5] was used here to achieve convergence and force the error function to zero, by allowing the phasor currents to more closely approximate their true values on successive iterations. After the rth iteration of the loop, consider the current in the Jth branch

$$i_{J_r}(t) = \sum_k i_{J_r}(k\omega) e^{jk\omega t}$$

with corresponding

$$\overline{i_{J_r}}(t) = \sum_k \overline{i_{J_r}}(k\omega) e^{jk\omega t}.$$

The next iteration is then carried out with $\overline{i_{J(r+1)}}(k\omega)$ formed by

$$\overline{i_{J(r+1)}}(k\omega) = p i_{J_r}(k\omega) + (1-p)\,\overline{i_{J_r}}(k\omega)$$

where p is determined by convergence considerations and $0 < p \leqslant 1$. Hicks and Khan and other authors [6] have investigated various criteria for convergence.

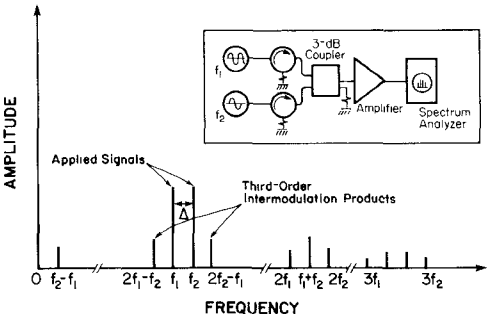

Fig. 2. Experimental setup for the measurement of two-tone intermodulation distortion in an amplifier. Two closely spaced tones at frequencies f_1 and f_2 are used as drive. The third-order intermodulation products are at frequencies $(2f_1 - f_2)$ and $(2f_2 - f_1)$.

III. The Modified Harmonic Balance Method

The harmonic balance technique described is an efficient and powerful tool for nonlinear analysis, particularly for distributed circuits, but is restricted to circuits with single-frequency or harmonically related inputs. This is because the DFT produces coefficients corresponding to discrete frequency components, which have frequency spacing $\Delta\omega = 2\pi/LT_s = \omega$. For $L = 2q+1$, there are q of these components, allowing the fundamental and its q harmonics to be efficiently extracted from the L uniformly spaced time-domain samples of the nonlinear current.

Fig. 2 shows a circuit which is used to determine the intermodulation distortion response of an amplifier. Two tones of slightly different frequency are superimposed at the input of the amplifier. Nonlinearities in the amplifier response produce additional spectral components at the output. In the analysis of this circuit, which has two nonharmonically related inputs at frequencies ω_1 and ω_2, the interval between the discrete frequency components from the DFT must be $\Delta = \omega_2 - \omega_1$ to ensure that all input signals (and any mixing products generated by the nonlinearity) are among the output discrete spectral components. A $2(q\omega_2)/\Delta$-point sequence of periodically spaced time samples is thus required to produce DFT spectral components at $0, \Delta, 2\Delta, \cdots, \omega_1 - \Delta, \omega_1, \omega_2, \omega_2 + \Delta, \cdots, q\omega_1, q\omega_1 + \Delta, \cdots, q\omega_2$. For small frequency differences Δ (e.g., a microwave intermodulation measurement), this is an enormous number of samples and beyond the numerical accuracy of most computers, since the number of operations needed in any DFT operation increases faster than N [7]. The modified harmonic balance (MHB) approach [8] is a variant of the harmonic balance method which permits efficient determination of all frequency components for small Δ.

The modified harmonic balance method uses the bandpass sampling theorem, which states that if a band-limited signal lying between $f_0 - B/2$ and $f_0 + B/2$ is placed suitably above the origin at f_0, the signal waveform may be completely reconstructed from time-domain samples of the signal taken at a rate $2B$ if f_0 is known. An analogy is the operation of a spectrum analyzer, where down conversion of the signal at f_0 to baseband allows the signal to be sampled at a lower (bandpass) frequency.

Consider the analysis of a waveform containing intermodulation components, i.e., one containing spectral components at $2f_1 - f_2$, f_1, f_2, and $2f_2 - f_1$. If the signal were band-limited to these four components, it could be completely represented by a nine-point (two times four components plus one) sequence of samples suitably chosen. Unfortunately, nonlinearities which produce sidebands at $(2f_1 - f_2)$ and $(2f_2 - f_1)$ from inputs at f_1 and f_2 will also produce components at $f_2 - f_1$, $3f_1$, and $3f_2$. These components occur because the nonlinear circuit may be analytically represented by a power series of at least third order. Substitution of a simple two-sinusoidal input into this power series will produce additional frequency components not present in the input. These components are extracted from the time samples at the output by the DFT, and must be applied to the hybrid matrix representing the linear circuit. Depending on the linear circuit, it is not until *then* that these components are reduced to negligible levels. Consequently, the desired band around f_1 and f_2 from which we seek the level of intermodulation components is NOT band limited to $(2f_1 - f_2)$ to $(2f_2 - f_1)$. Bandpass sampling the (broad-band) time-domain waveform produced by the nonlinearity will result in aliasing and incorrect computation of the desired components.

The process of aliasing may best be described mathematically. If $X_s(e^{j\omega})$ is the DFT of a sequence x_n $(n = 0, 1, \cdots, N)$ obtained by periodic sampling of a time-domain waveform $x(t)$, i.e., if

$$x_n = x(nT_s) = \frac{1}{N} \sum_{k=0}^{N-1} X_s(e^{jk\omega}) e^{jnk\omega}$$

where T_s is the sampling interval and $\omega = 2\pi/N$, then $X_s(e^{j\omega})$ may be found by assuming that the sequence x_n is periodic on N and is given by

$$X_s(e^{jk\omega}) = \sum_{n=0}^{N-1} x_n e^{-jnk\omega}.$$

A property of the DFT is that

$$X_s(e^{j\omega}) = \frac{1}{T_s} \sum_{r=-\infty}^{\infty} X_a\left(\frac{j\omega}{T_s} + \frac{j2\pi r}{T_s}\right) \qquad (3)$$

where $X_a(f)$ is the (analog) continuous Fourier transform of $x(t)$ [7]. $X_s(e^{j\omega})$ is periodic in ω, and the baseband interval $-\pi < \omega < \pi$ is indistinguishable from other bands spaced at higher multiples of π. Aliasing occurs in the DFT whenever T_s is so large that the increment $2\pi/T_s$ by which X_a is linearly translated in (3) is sufficiently small to cause successive shifts of the band to overlap. This occurs if

$$\frac{2\pi}{T_s} < (2B)2\pi, \qquad \text{i.e., } T_s > \frac{1}{2B} \qquad (4)$$

where B is the total signal bandwidth and the factor $2B$ accounts for both positive and negative shifts of the band. Fig. 3 demonstrates the effect of successive linear shifts on X_a to produce X_s. Overlap between successive shifts does not occur because T_s equals the limit given in (4). Restated,

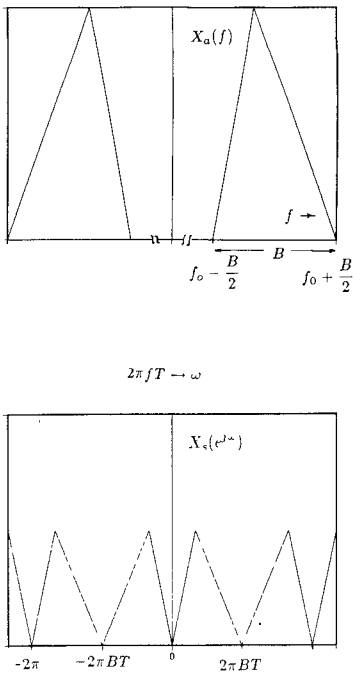

Fig. 3. Comparison between the continuous Fourier transform $X_a(f)$ (top) and the DFT $X_s(e^{j\omega})$ (bottom). Sampling the time-domain waveform represented by $X_a(f)$ at a rate $T_s = 1/2B$ results in the periodic translation and scaling shown to produce $X_s(e^{j\omega})$.

aliasing will not occur if the sampling frequency $1/T_s$ is at least twice the bandwidth B of the band-limited spectra. The above discussion assumes that the bottom edge of the bandpass B is an integral multiple of $2B$ above the origin. Slight shifting of the chosen bandwidth may be necessary to achieve this. The bottom edge of the band will be referred to as the bandedge in the following discussion, where it is assumed to satisfy this criterion.

Consider the application of the bandpass sampling theorem to the waveform represented by the spectrum in the top of Fig. 4(a). Choose a bandwidth B of interest lying between $f_1 - 2\Delta$ and $f_2 + 1.5\Delta$, so that $B = 4.5\Delta$ and the bandedge is at $f_1 - 2\Delta$. The aliasing resulting from bandpass sampling a non-band-limited signal is easily derived using (3) and considering the translation of X_a resulting from various r. The beat frequency at $f_2 - f_1$ will be translated by integral multiples of $2B$ upon sampling if $T_s = 1/2B$. For the zero-translation case, the beat component will remain in its frequency slot at Δ. When downshifted $(f_1 - 2\Delta)/2B$ times, the component at $f_1 - \Delta$ will also occupy the frequency slot at Δ. Since the sampled frequency spectrum is given by (3) as the sum of the analog spectra shifted by all possible periodic translations, the component given by the DFT as the fundamental frequency at Δ will not be the lowest order intermodulation product (that at $(f_1 - \Delta)$ downshifted) alone, but will be this component summed with the beat-frequency component. The bandpass sampling theorem is not truly applicable in this instance because the signal being sampled is not truly band limited to the region of interest (i.e., $(f_1 - 2\Delta)$ to $(f_2 + 1.5\Delta)$).

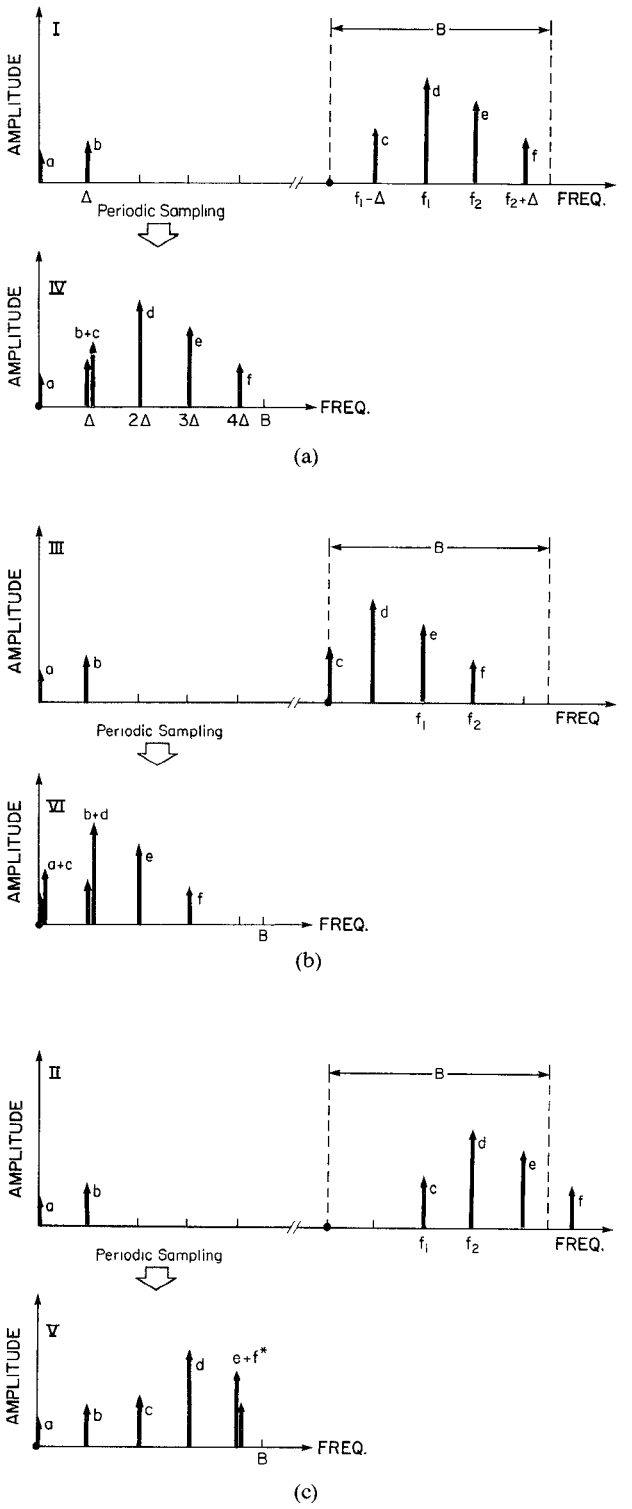

Fig. 4. Sequence of shifts used for a simple waveform in order to de-embed the aliasing. Here, d and e are the two fundamental output signals corresponding to the two applied input tones. (a) $X_a(f)$ at the output of the nonlinearity (top). The time-domain waveform corresponding to $X_a(f)$ is sampled at a bandpass rate. The baseband spectral components $X_s(f)$ produced by application of the DFT to the sampled sequence are shown at the bottom of the figure. (b) Same as (a), but the two applied input signals have been translated down by Δ. The output spectrum $X_a(f)$ is correspondingly shifted. Different aliasing results, giving $X_s(f)$ at the bottom of the figure. (c) Same as (a), but the two applied signals have been translated up by Δ. (d) The three discrete output spectra $X_s(f)$ resulting from applied input signals at f_1 and f_2 (top), $f_1+\Delta$ and $f_2+\Delta$ (middle), and $f_1-\Delta$ and $f_2-\Delta$ (bottom).

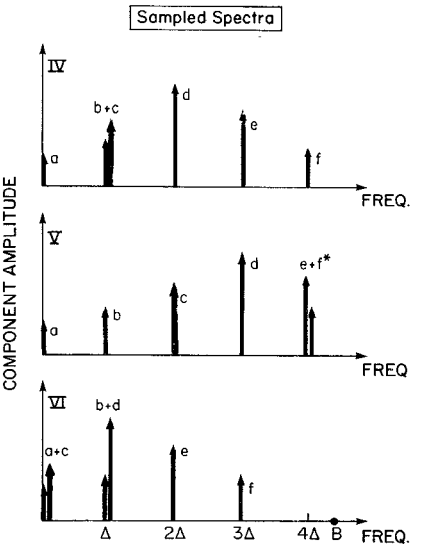

(d)

Fig. 4. Continued

A. Controlled Aliasing

Two observations are pertinent to bandpass sampling. The first is that although considerable aliasing occurs by selecting a band window surrounding the desired spectral components and sampling at the slow bandpass rate ($T_s = 1/2B$), most of the components at spacings Δ between the beat frequency and the lower bandedge are zero and thus do not contribute to the sampled spectrum. The second observation is that the exact frequencies of the nonzero components contributing to aliasing can be determined, and their location in the aliased spectrum easily found. This suggests the use of *controlled aliasing* to determine the magnitude of these components.

Consider again the top waveform of Fig. 4(a). Periodic sampling of the time-domain signal at the bandpass rate and applying the DFT results in the aliasing shown in the bottom of the figure, where the components labelled b and c overlap in the spectrum obtained. Setting $r = 0$ in (3) yields the components labeled a and b at frequencies 0 and Δ. Setting $r = +(f_1 - 2\Delta)/9\Delta$ translates the components c, d, e, and f into the frequency slots at Δ, 2Δ, 3Δ, and 4Δ, respectively. The discrete spectrum X_s is the sum of the spectra corresponding to these two values of r, as shown in the bottom of the figure. Other values of r will also translate $X_a(f)$, but will add in null components to these frequency slots. Due to the periodicity of X_s, the baseband interval between 0 and 4.5Δ completely describes the remaining translations, and hence X_s. The magnitudes a, d, e, and f can be directly determined from the Fourier coefficients, but only the total magnitude of $(b+c)$ is known.

The heart of the controlled aliasing technique lies in the solution of the remaining unknown magnitudes by simple, linear algebra. Suppose the same two input signals of relative magnitude d and e are applied to the system, as before, but at frequencies shifted down by Δ to $f_1 - \Delta$ and

f_1, as shown in Fig. 4(b). For a low-Q device model (i.e., one in which the output signals do not vary rapidly with slight frequency changes in the input signal, as for a resistive nonlinearity), the output component magnitudes a through f will be essentially unchanged. However, their frequencies will be altered according to the order of the nonlinearity that created them. Now the intermodulation products will lie Δ lower than in the unshifted case, but the beat frequency at Δ will be unchanged. Furthermore, because the position of the applied signals relative to the bandedge has been changed, different aliasing will occur. In this case, when $r = +(f_1 - 2\Delta)/9\Delta$ in (3), the bandedge, now occupied by the component c, will overlap with the dc component to give a total component $(a + c)$ at zero frequency (dc). The component at $f_1 - \Delta$, now of value d, will overlap with the beat component b at Δ to give a total Fourier coefficient at Δ of amplitude $(b + d)$. Since a and d are known from the first application of the DFT, the value of the components b and c can be directly obtained by simple subtraction. Fig. 4(c) shows an alternate frequency shift (a translation up by Δ) that could also be used, and the baseband interval of the resulting aliased spectra X_s. Fig. 4(d) summarizes the DFT spectra obtained from the three cases. Each is different.

The following generalizes the procedure for each node when the band window is chosen to contain P discrete spectral components (including the bandedge, which translates to dc): by sampling the time-domain nonlinear current waveform at a very slow bandpass rate, P Fourier coefficients can be obtained from the DFT. By frequency-shifting the two input signals by Δ, recalculating the time-domain waveform, and resampling, P additional, different Fourier coefficients can be obtained from the DFT. If the frequency translation, sampling, and DFT are repeated m times, a total of mP Fourier coefficients are obtained. Because the way in which the new frequency components will alias is known, a system of mP linear algebraic equations can be obtained relating the unknown component magnitudes to the DFT coefficients obtained. By inverting the system of equations just once, the unknown amplitude of all frequency components can be obtained by applying the inverse matrix to the DFT coefficients obtained after m translations.

B. Solution for the Unknown Components

In the simplified example given, just two frequency shifts were required, since only six frequency components were present. The formulation and selection of independent equations and their solution for the unknown amplitudes were trivial in this case because all higher components were ignored. If two input signals (of two different frequencies) are applied to an analytic fifth-order nonlinearity, 31 frequency components (including dc) are present in the output signal, and the band window of interest will consist of six signals, each spaced by Δ (two fundamental and two each of third- and fifth-order intermodulation products). For bandpass sampling, a 13-point sequence of samples spaced unformily $1/13\Delta$ in time (corresponding to $B = 6.5\Delta$) may be used to extract the signals of interest. Since seven real and six imaginary Fourier coefficients will be obtained from each 13-point sequence (dc, $\Delta, 2\Delta, \ldots, 6\Delta$ and $P = 7$), a minimum of $m = 5$ frequency shifts of the input signals is needed to ensure that a sufficient number of equations is obtained to permit solution of all 31 unknowns. However, these equations do not necessarily form an independent basis. To form a set of 31 *linearly independent* equations relating the real unknowns and the real part of the Fourier coefficients, a total of $m = 6$ translations is needed. This gives a selection of 42 equations, from which 31 linearly independent equations must be chosen. An additional set of 30 equations is then selected to relate the imaginary components. The imaginary set contains one less equation than the set needed to solve for the real parts because the dc component has no imaginary part.

Other solutions exist to de-embed the aliasing. The example above uses a bandwidth of 6.5Δ and calculates the Fourier coefficients from a sequence of 13 time samples sampled at a bandpass rate. An alternative approach would be to open the band window of interest beyond 6.5Δ so that fewer than six frequency translations would be required (i.e., increase P and reduce m). This would open up more vacant slots and simplify the aliasing, but would require more time samples for the DFT and be less computationally efficient. Alternatively, certain symmetry properties could be applied. If the two input signals were always of equal level, the intermodulation products and harmonics would also be of the same amplitude, and the number of unknowns would be reduced by half [9]. This approach was rejected here to enable the two input signals to be of any (differing) arbitrary magnitude.

IV. Implementation of the Modified Harmonic Balance Procedure

Several modifications are needed in the standard harmonic balance software to allow for the additional frequency shifts required to de-embed the aliased amplitudes. No changes are needed in the DFT algorithm which performs the time-sample-to-frequency conversion, but the algorithm to perform the phasor (frequency)-to-time conversion must be altered to account for the different frequency translations. During each iteration of the harmonic balance loop, step 3) must now incorporate the six frequency translations to calculate the six sets of time samples sampled at a bandpass rate. Step 5) must perform a DFT on each set to calculate the Fourier coefficients, and finally perform the inverse matrix multiplication to de-embed the desired phasor current components. The error function in step 6) is then calculated as an amplitude error sum based on the frequency components that are considered predominant. In the FET examples that follow, 11 components (out of a total of 31) were included: the dc, fundamentals, second harmonics, third harmonics, and the third- and fifth-order intermodulation products. The minimization is attempted by adjusting their values accordingly. Looping back to step 2), the updated current esti-

mates are reapplied to the linear circuit to calculate new phasor voltages (at the 11 predominant frequencies) to reimpress upon the model. The effect of additional higher order frequency products resulting from the multiple-frequency input is neglected.

The efficiency of the MHB technique is impressive. Six sets of frequency translation requiring 13 time samples each are needed; i.e., 78 calculations are required of the nonlinear model to de-embed all 31 frequency components. This is an improvement of several orders of magnitude over the brute-force Byquist method, which for $f_1 = 10$ GHz and $\Delta = 1$ MHz would have required 30 000 time samples to achieve the same result.

A. Limitations of the Technique

The MHB technique is the first reported application of the harmonic balance method which is able to analyze nonharmonically related signal excitations in a nonlinear circuit of potentially any complexity [8]. Although other solutions have since emerged [10], this method remains the simplest for the analysis of intermodulation distortion, resistive mixers, and small-signal gain suppression in nonlinear systems.

The method was implemented assuming a nonlinearity of fifth order or less. Higher order frequency products will cause aliasing that has not been accounted for and will not be de-embedded. This occurs at larger signal strengths, at which the higher order nonlinearities become significant. In theory, de-embedding could be achieved for any desired nonlinearity by increasing the band window. Fortunately, signal strengths at which unaccounted for aliasing becomes a problem can be detected by output asymmetry when a symmetrical input waveform (one which has two equal level tones) is applied.

The principal limitation of the method is that the device must be low-Q, so that the frequency translation does not affect the magnitude of the frequency component that we seek. The frequency translation affects only the nonlinear circuit and not the linear one. This poses no problem if the nonlinearity is purely resistive, or if any frequency-dependent elements in the model can be linearized and partitioned into the linear circuit. However, for reactive nonlinearities, the small frequency translation can produce minute changes in the signal amplitude. Unfortunately, these changes are comparable to the level of many of the components we are seeking to de-embed (e.g., the intermodulation products). This phenomenon predominates at extremely low signal levels when numerical resolution is poor, and can also be detected by asymmetry in the output spectrum produced by two equal-level input signals. The effect is eliminated by choosing an extremely narrow signal spacing relative to the carrier frequency. In the calculation of intermodulation distortion and gain suppression, this is not a major problem, as the intermodulation products have been experimentally observed to be independent of frequency separation [11]. Other intermodulation analyses such as analytical methods [12], [13] or Volterra series [14] also neglect the frequency dependence of the signal separation.

B. Testing the Modified Harmonic Balance Method

The MHB method was implemented in FORTRAN on an IBM AT Personal Computer. The required memory for the algorithm was 120K, with an additional 70K needed when compiled with the physical FET model reported by Madjar and Rosenbaum [15]. Run time was approximately 2 min for each solution. This is the first report of a harmonic balance technique implemented on a desktop personal computer. The strength of this implementation is that it allows complete nonlinear, steady-state analysis of circuit–device interactions at a computer workstation.

The most useful check of nonlinear performance is to apply an input signal of the form

$$V = (a\cos 2\pi f_1 t + b\sin 2\pi f_2 t)$$

to a fifth-order nonlinearity such as

$$I = V + V^2 + V^3 + V^4 + V^5$$

and solve for the frequency components of I. The use of two unequal signals levels a and b forces asymmetry in the spectrum, and the use of cosine and sine terms checks both the real and imaginary de-embedding. Analytical substitution of V into the expression for I is surprisingly complex. For instance, the dc component equals

$$\frac{3a^4}{8} + \frac{3b^4}{8} + \frac{a^2+b^2}{2} + \frac{3a^2b^2}{2}$$

while the intermodulation component at $(2\omega_1 - \omega_2)$ varies sinusoidally with magnitude

$$-\frac{1}{2}\left[\frac{3}{4}a^2b(a^2+b^2) + ab\left(a + \frac{3}{4}a^3 + \frac{3}{2}ab^2\right) + \frac{a^2}{2}\left(b + \frac{3}{2}a^2b + \frac{3}{4}b^3\right) + \frac{3}{4}a^2b^3 + \frac{1}{4}a^4b + \frac{3}{8}a^2b^3\right].$$

Convergence was obtained very quickly in the test cases because all the parasitics in the external circuit were removed. A value of $p = 0.9$ reduces the error function by 10^{-2} each iteration. Computed values were as expected, with relative errors in each component less than 10^{-6}.

V. Examples of Nonlinear Circuit Design

Several examples illustrating the usefulness of the method are presented below.

A. FET Frequency Doubler Design

FET frequency doublers are important components in microwave receivers. Wide-band doublers minimize local oscillator requirements in phase-locked loops and tracking systems because they provide a simple means of generating higher frequency components.

Several design techniques for frequency doublers have previously been reported [16]–[19]. The design presented here uses single-gate MESFET's and standard MIC techniques, and uses the nonlinearity of the FET transcon-

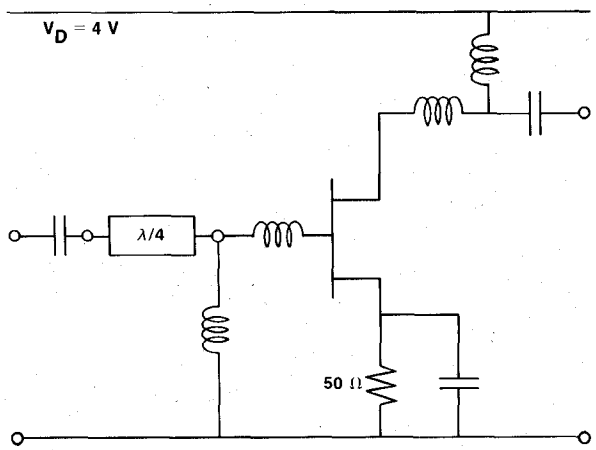

Fig. 5. Circuit topology of the nonlinear FET element (harmonic generator) used with the broad-band doubler.

ductance to achieve doubling. The circuit inherently rejects the fundamental and odd-order harmonics over bandwidths greater than an octave. The bandwidth of the doubler is limited only by the bandwidth of the Lange couplers used at the FET input and output.

One difficulty in designing a doubler covering octave or greater bandwidths is that the highest frequency in the band to be doubled will overlap with the desired (second-harmonic) output of a lower frequency input. Consequently, the traditional approach of tuning the FET input to the fundamental frequency and tuning the FET output to the second-harmonic frequency will result in compromised performance at the bandedges.

The second design difficulty lies in optimizing the FET operating point to achieve maximum conversion efficiency, i.e., to optimize circuit interaction with the device nonlinearity. Tradeoffs between FET gain and harmonic conversion efficiency are difficult to characterize.

This example describes how the nonlinear design technique can be used to synthesize the desired circuit and to set the device bias and RF operating point, and illustrates the circuit approach used to obtain inherently broad-band operation. Two considerations are accounted for in the design approach; the first is that conversion loss be as low as possible, and the second is that the fundamental signal be rejected. Using conventional approaches, that is particularly hard to achieve for a 4–8-GHz doubler at 8 GHz, as this frequency is both the doubled 4-GHz signal and a possible fundamental input.

The input and output circuits of the basic FET doubler stage were synthesized for maximum flat gain across the whole band using standard small-signal techniques. The circuits can then be verified at small-signal levels with the nonlinear algorithm and model. Unlike conventional single-frequency doublers, however, the wide-band input and output matching circuits must be low-Q to maximize bandwidth. The FET's used were NE71000.

The circuit topology for the nonlinear element chosen is shown in Fig. 5. Using the MHB program with only a single input frequency, the (small-signal-derived) matched

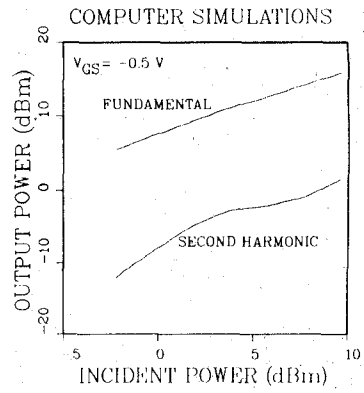

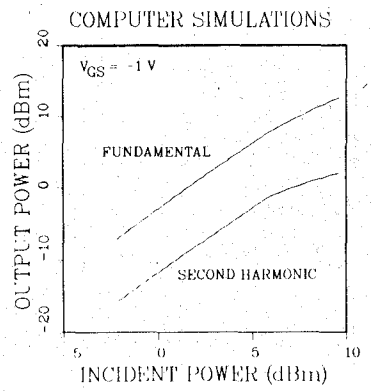

Fig. 6. Modeled results of the nonlinear FET element of Fig. 5. Simulations of fundamental and second harmonic output power are shown as a function of fundamental input power at (a) $V_{GS} = -0.5$ V and (b) $V_{GS} = -1.0$ V. Drain–source voltage was 4 V.

FET stage was analyzed for doubling efficiency at various device bias and RF drive points. The model used has been previously reported [20], and contains a three-terminal nonlinear capacitance in addition to nonlinearities in g_m and g_D. Optimum conversion efficiency was obtained by setting the device bias near pinchoff, using an RF-bypassed 50-Ω resistance in the source. Biased in this fashion, the FET behaves as a harmonic generator. Modeled simulations of fundamental and second-harmonic output power at 8-GHz input are shown in Fig. 6. By varying the source resistor, the gate–source bias voltage can be changed. From the figure, optimum second-harmonic to fundamental output power is achieved with a gate bias of -1 V and an incident power around 5 dBm.

1) Circuit Topology: Although optimized for second harmonic generation, the level of the fundamental frequency at the single-stage FET output is still approximately 10 dB greater than the desired second harmonic. The single-stage doubler just described has no rejection, because rejection would result in poor conversion performance at the lower edge of the output band (which corresponds to the upper edge of the input band in an octave bandwidth design). In this application, the FET is used solely as a nonlinear element for generation of a second

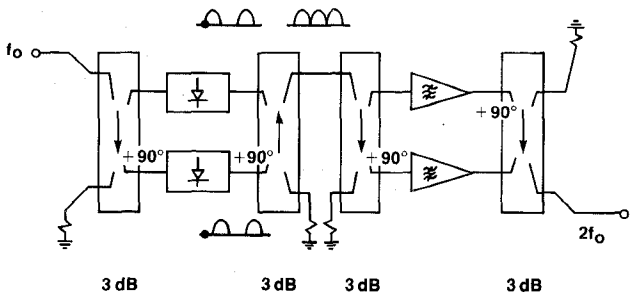

Fig. 7. Construction of the broad-band doubler. The initial block comprises a pair of nonlinear FET harmonic generators coupled by two antisymmetric Lange couplers to provide a 180° path difference. The final block is a balanced bandpass amplifier that uses symmetrically coupled Lange couplers to provide zero net phase difference.

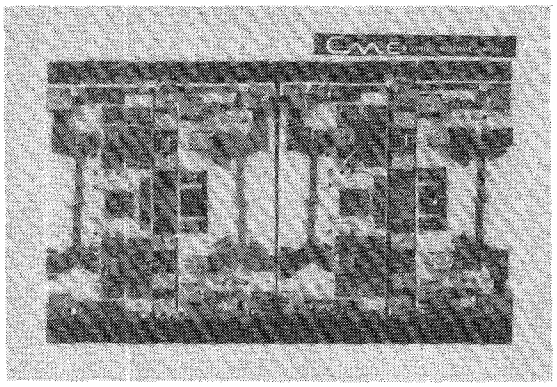

Fig. 8. Photograph of the broad-band doubler. The input is in the lower left corner of the figure.

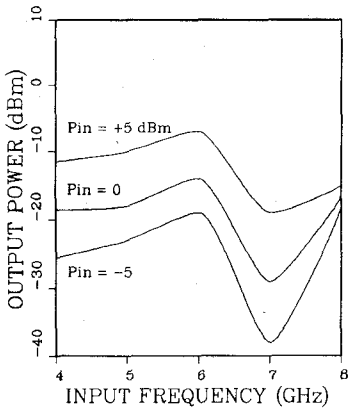

(a)

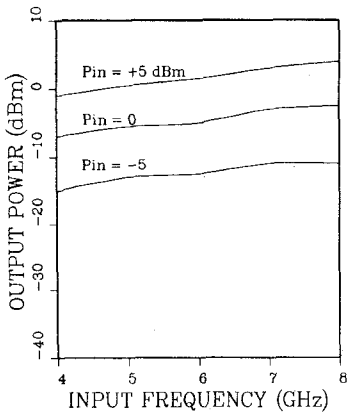

(b)

Fig. 9. Measured doubler results, showing the (a) fundamental and (b) second-harmonic output power as a function of frequency, for input power levels of −5, 0, and +5 dBm.

harmonic and behaves like a half-wave rectifier. Any stable device with sufficient microwave gain could be used in place of the FET. For example, Schottky diodes could be substituted for the FET's in order to generate a second-harmonic signal.

Fundamental frequency rejection is achieved by two means.

The first involves coupling two FET half-wave rectifiers antisymmetrically, so that conduction occurs on alternate half-cycles, as illustrated in Fig. 7. Two Lange couplers, oriented to provide a total path difference of 180°, are ideal for this purpose, as they allow isolation between the two half-circuits and provide good input and output VSWR over the necessary bandwidth, in addition to the required phase difference. The antisymmetric configuration effectively nulls out the fundamental and odd-order harmonics, because the 180° phase shift difference results in pure cancellation (subtraction) of the odd-order frequencies.

The other way of achieving fundamental frequency rejection is by adding a following band-reject amplifier. Additional cancellation of the fundamental is achieved in this balanced amplifier stage, as its Lange couplers are designed for the midrange of the output band and reject the input band. In addition, the amplifier itself provides gain at the second harmonic and rejection at the fundamental. Conventional small-signal techniques were used to synthesize this stage.

1) Results: The circuit in Fig. 7 was fabricated on a 0.015-in alumina substrate and used Lange couplers centered at 12 GHz. The complete doubler is shown in Fig. 8. Circuit size was 0.5 in. by 0.25 in. and power consumption was 60 mA at 4 V input.

Measured doubler results are illustrated in Fig. 9. Input drive level of +5 dBm was found to give the highest conversion efficiency, close to that determined in the simulations. The second-harmonic output power was tuned to rise slightly over the band to compensate for following system losses. At 16 GHz, a peak output power of +4 dBm was achieved, for a total conversion loss of 1 dB. Rejection at the fundamental frequency was 20 dB. Maximum conversion loss of 6 dB was obtained at 8 GHz, with fundamental frequency rejection of 15 dB. Fundamental rejection was highest around 7 GHz due to a perfect phase and amplitude balance in the input and output Lange couplers at this frequency.

B. Reduction of Intermodulation Distortion in a Power Amplifier

Intermodulation distortion is an undesirable effect in communications amplifiers because it introduces a form of crosstalk into the channel, as band-limited signals can

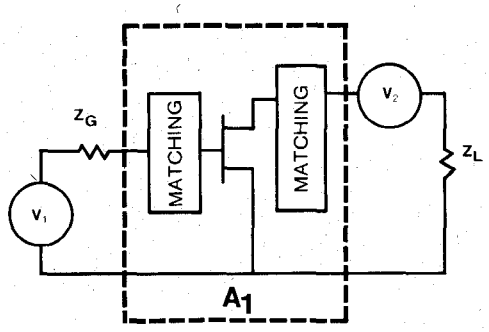

Fig. 10. Linear amplifier topology used in the MHB simulations for reduction of intermodulation distortion.

interact with any odd-order nonlinearity to produce additional frequency components that fall within the band. The new components are known as intermodulation products, and limit the level at which linear amplifiers can operate. As input power is increased, the stronger nonlinearities in the transfer characteristic of the amplifier become significant and produce spectral components that can interfere with the desired signal.

One of the principal advantages of the MHB method is its ability to predict the effect of circuit–device interactions on the level of the third-(and higher)-order intermodulation products. A two-tone intermodulation test is able to identify amplifier nonlinearity far more easily and accurately than simple one-tone tests of compression and AM/PM, in which small deviations from linear gain or phase must be observed. The typical two-tone test uses apparatus similar to that shown in Fig. 2, where two closely spaced signals of equal level are impressed upon the device input. The level of the fundamental and intermodulation products are observed as a function of input power to give a measure of the system nonlinearity.

Intermodulation distortion can be reduced by careful design techniques. Many of these may be investigated with the MHB technique. For instance, in an FET amplifier, 5-dB reduction of the third-order intermodulation product may be achieved by simply ensuring that the second-harmonic terminating impedance at the gate is a short circuit. This prevents any second-harmonic voltage being reimpressed upon the FET and mixing with a fundamental input to produce an in-band distortion product. Other means that have previously been investigated [20] include raising the drain voltage or introducing some feedback resistance.

A novel scheme was discovered during simulations with the model. Fig. 10 illustrates the concept. Amplifier A_1 is a matched FET amplifier driven *simultaneously* by applied voltages V_1 and V_2, where V_2 is a voltage injected into the FET drain. Simulations of this configuration were run using the MHB approach. (Note that for intermodulation simulations, both the signals V_1 and V_2 actually consist of two tones each.) An increase in the output power resulted. Even though the FET inverts voltage V_1 at the drain so that if V_2 is of similar phase to V_1 the total RF drain-voltage swing is reduced, the current is increased and the phase angle between the voltage and current at the output

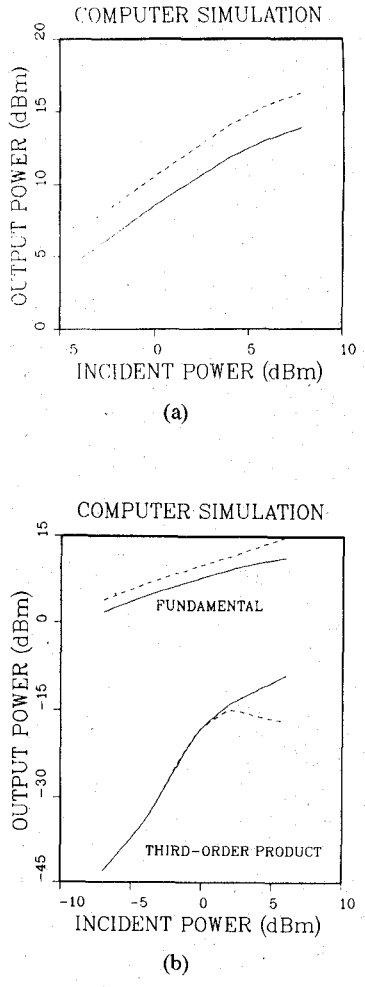

Fig. 11. (a) Single-tone simulation of linear amplifier response as a function of input power showing fundamental output power for $V_2 = 0$ (solid) and $V_2 = V_1$ (dashed). (b) Two-tone simulation of linear amplifier response and third-order intermodulation-distortion product as a function of input power. Amplifier topology is shown in Fig. 10. The solid curve shows response for $V_2 = 0$; the dashed curve for $V_2 = V_1$.

is reduced, so that the net output power actually increases. Additionally, the reduction in output voltage swing reduces the level of the third-order intermodulation distortion. The voltage reduction is associated with the reactive part of the load trajectory; the overall effect is similar to an active load-pull, where the added voltage V_2 provides a form of dynamic tuning at the output in such a way as to reduce distortion.

Computer simulations are shown in Fig. 11 for a low-power prototype amplifier that used FET's with a gate width of 400 μm. Both V_1 and V_2 were set equal in amplitude and phase in the simulations used to derive Fig. 11(a) and (b), which are one-tone and two-tone power curves respectively. The uppermost curve (dashed) in each graph is the fundamental output power in the new system. The solid curve indicates, for comparison, the modeled response of the original system with $V_2 = 0$. As can be seen, the distortion reduction effect occurs at high power levels, where the distortion products are reduced by up to 10 dB. Furthermore, because of the increased output power, the ratio of output power to intermodulation distortion

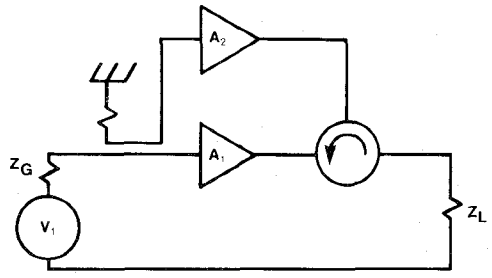

Fig. 12. Discrete implementation of the linear amplifier of Fig. 10.

(C/I) is considerably increased. At an output power of 5 dBm, for example, the ratio has improved from 39 dB to 45 dB. At higher power levels, where the third-order product begins to reduce, the improvement is substantially greater.

The implementation of this scheme is very difficult using discrete parts, and could be attempted more simply monolithically. A discrete implementation is shown in Fig. 12. There, the signal V_2 is generated by coupling some of the input signal V_1 into a secondary *linear* amplifier A_2, and injecting the new signal into the output of the original amplifier A_1. It is important to note that this is not a feedforward scheme, where amplifier A_2 would be nonlinear and used to generate distortion components that are subtracted from those produced by A_1. In this case, a *linear* in-phase reproduction of the input signal (assumed pure) is added to the output voltage produced by the FET. In order to add the voltage V_2 in series with the drain output, a circulator was used. The resultant combined voltage is then circulated to the output load. To match the simulations, this would require that A_2 have zero source impedance and produce an internal voltage swing of V_2 equal to V_1. Since the outputs of both A_1 and A_2 were internally matched to 50 Ω, the voltage added by A_2 was actually $V_2/2$ if V_2 is the internal output voltage of A_2. In a monolithic implementation, A_2 could be designed with low output impedance and act as a voltage source to A_1 to overcome this difficulty.

In its practical implementation, an NEC NEZ5964-6 6-W power FET was driven as part of a 50-dB gain amplifier chain. To supply the injected RF drain voltage, an 8-dB branch-line coupler and an NEC NEZ5964-3 3-W device were used as amplifier A_2. Fig. 13(a) shows the measured intermodulation distortion spectrum of A_1 alone driven with two signals of +34 dBm each at the output. Fig. 13(b) shows the spectrum when A_2 is added; third-order products are reduced by 8 dB and fifth-order products by over 20 dB. Simple power combining of the NEZ-3 with the NEZ-6 would theoretically reduce the third-order products alone by only 3.5 dB. Relatively narrow bandwidths (100 MHz) were achieved because of the discrete, internally matched components used.

The phase of V_2 relative to V_1 can be varied through any phase angle in the simulations. As it is rotated through 90° to 180°, the opposite effects are observed: lower output

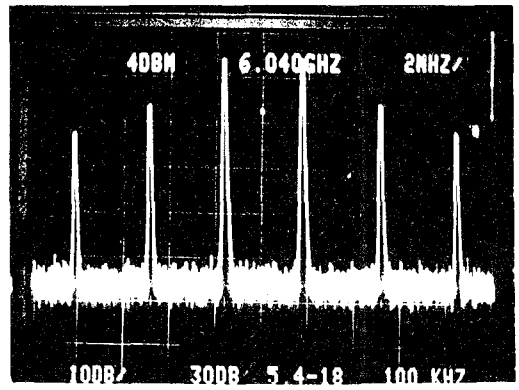

(a)

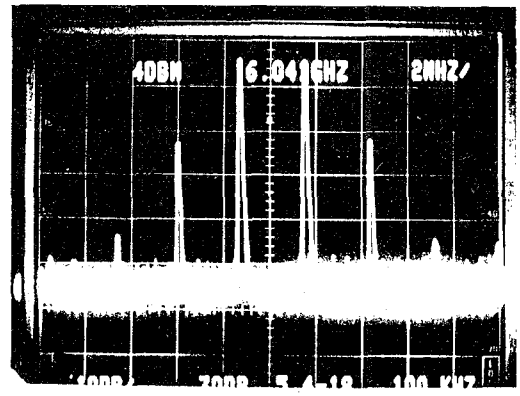

(b)

Fig. 13. Measured intermodulation spectrum of a 6-W power amplifier with two output signals of +34 dBm each at the output. (a) Without signal injection at the drain. (b) With signal injection at the drain. Vertical scale is 10 dB per division.

power, higher distortion products, and severely deteriorated power-to-distortion ratio. Experimentally, phase tuning was achieved by using a variable-length microstrip line at the output of A_2.

In a typical power-combined amplifier using a 3-dB hybrid at its output, the output powers of two identical FET's are combined to increase output power. Consequently, a 3-dB improvement in intercept point is achieved, with a theoretical improvement in C/I of 6 dB due to the back-off possible in operating with lower output power. The scheme presented here also employs a type of power combining, but the FET's need no longer be of equal power-handling capability. For the additional cost of a coupler and a circulator, considerably greater improvement in C/I can be achieved compared to power combining amplifiers, due to the improved linearity obtained by using vectorial addition of the output voltages to dynamically tune the FET. Such a scheme could be more efficient than either present predistorter or "back-off" approaches.

C. Gain Suppression in Limiting Amplifiers

A phenomenon that has been known for a considerable time in limiting amplifiers [21], [22] and nonlinear ampli-

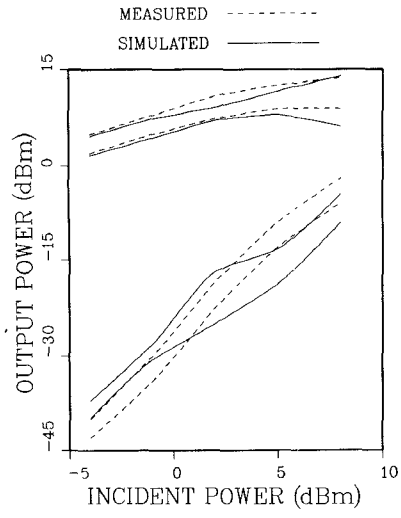

Fig. 14. Two-tone tests of the FET feedback amplifier. Two unequal level tones of level P_{IN} and $P_{IN}-3$ dB were applied. The top set of measured and simulated curves shows the output power in each fundamental carrier; the bottom set shows the level of each third-order intermodulation sideband. Measured curves are dashed; simulated are solid.

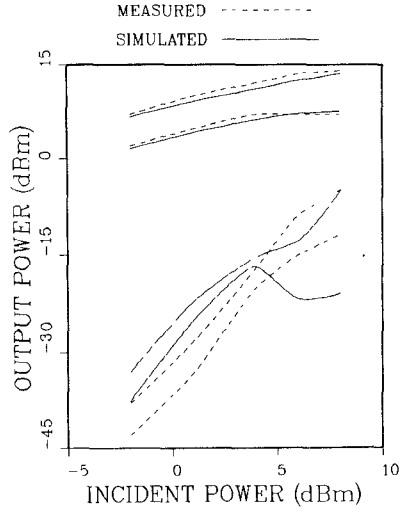

Fig. 15. Same as Fig. 14, but with two applied tones of level P_{IN} and $P_{IN}-5$ dB.

fiers [23] is the possible improvement of 3 dB in the output signal-to-noise ratio of a signal which is much stronger than the noise. A consequence of this result is that, for large signal-to-noise ratios, the output power ratio of a weak signal to a much stronger (simultaneous) signal at a different frequency in the band can be up to 6 dB less than the same ratio at the input of the limiter or saturating amplifier. This is known as gain suppression of the weaker signal. The MHB method can be used to demonstrate this trend by performing an intermodulation analysis in which the two input tones are of *unequal* level. The advantages of this approach over previous analytical treatments of the phenomenon are that the nonlinearity is a dynamic function of the instantaneous operating point of the device (because a device model is used), and that the frequency components are obtained numerically.

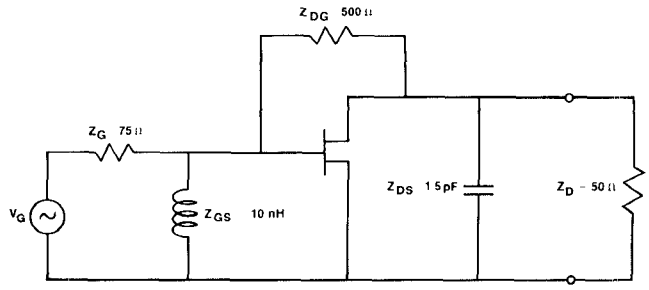

Fig. 16. Lumped element equivalent circuit model of the FET feedback amplifier used in the gain-suppression experiments of Figs. 14 and 15.

Figs. 14 and 15 show both simulations and experimental results for the fundamental output power and third-order product in each of the two carriers and their sidebands. The simulations are shown as solid lines; the experiments as dashed. The amplifier used is illustrated in Fig. 16; it comprises an NEC 72083 FET embedded in a resistive feedback circuit, with a feedback resistor of 500 Ω. The FET was biased at $V_{GS}=-0.25$ V and $V_{DS}=3$ V, and driven well into saturation by two tones at the gate of frequency 2.000 and 2.001 GHz. The horizontal axis in Figs. 14 and 15 represents the power incident in the strongest signal. In Fig. 14, the smaller incident signal is 3 dB weaker than this; in Fig. 15, it is 5 dB weaker. In both cases, the small-signal gain is 9 dB. At an incident power of +8 dBm for the strongest signal, the amplifier is compressed, and the stronger signal output power is 14.3 dBm in Fig. 14 and 14.5 dBm in Fig. 15. In Fig. 14, the output power of the weaker signal (at 5-dBm incident power) is then just 9 dBm. Similarly, in Fig. 15, the weaker signal of 3-dBm incident power produces an output power of just 7 dBm. In both cases, the gain of the small signal has been suppressed by about 2.5 dB.

The measured behavior of the third-order intermodulation sidebands is also interesting. The difference in levels between the two third-order products is directly proportional to the level separation between the two input signals (3 dB and 5 dB, respectively). The simulations also show that the separation between the two second-harmonic signals is twice (in dB) the input signal level separation, and three times the input level separation for the third-harmonic outputs.

Agreement between the measured and simulated results is good. The amplifier used in the simulations was not an ideal limiting amplifier, but the onset of gain compression and saturation gave it similar characteristics. Unfortunately, an ideal limiting amplifier has nonlinear terms of infinite order, and the results obtained by this method would be in error due to the additional aliasing. By considering a "soft limiter," the MHB technique could be useful in the design of nonlinear amplifiers tailored for suitable gain characteristics. A predistorter is an example. The application of the technique to the analysis and design of resistive mixers is also straightforward, and is similar to the example just given.

VI. Conclusions

A technique that permits the investigation of device–circuit nonlinearities for two input frequencies has been presented. Using modifications to an existing FET model [15], [20], a harmonic balance method was devised which was efficiently implemented on an IBM PC-AT and which overcame the problems associated with a small frequency difference relative to the carrier frequency. By bandpass sampling the time-domain waveform generated by the FET model, and by small input frequency changes, the desired fundamental and intermodulation components can be reconstructed from the aliased spectrum. By achieving a harmonic balance between the frequency components present in the nonlinear model and the linear circuit, Kirchhoff's laws are satisfied. This enables the effect of circuit and device parameter changes to be determined for both single- and two-tone excitation. The method is numerically efficient because:

i) the linear circuit is analyzed by an N-port matrix in the frequency domain, where differing time constants correspond only to different amplitude phasor components, and additional branches do not increase the size of the matrix;

ii) the time-domain waveform from the model is sampled not at the Nyquist rate for two closely spaced signals, but at the bandpass rate; and

iii) the time-domain waveform is obtained as an explicit function of the input nodal voltages and their time derivatives.

The method in principle allows any nonlinear time-domain model to be used. The nonlinearity can be a function of the instantaneous (unknown) operating point; i.e., it can account for changing bias conditions. Harmonics and higher order frequencies generated are reimposed as additional inputs to the model, and a solution is obtained for the phasor value of every frequency component present, including dc components.

The restrictions on the method as implemented are that the nonlinearity be no greater than fifth order, and that if the nonlinearity is frequency-dependent (i.e., nonresistive), the frequency spacing of the two input signals be much less than the carrier frequency. The method gives results identical to the standard harmonic balance method for all nonlinearities whenever the input level of the second tone is set to zero.

Three novel examples of nonlinear circuit design have been presented. The first is of a novel FET frequency doubler, covering octave bandwidths. The MHB method was used with a single-tone input to set the device bias and operating points. The circuit structure is applicable to any microwave nonlinear device as the active element. Using single-gate FET's, conversion efficiencies of from -1 to -6 dB were obtained across the output frequency band of 8 to 16 GHz. The second was a technique which allows reduction of third-order intermodulation distortion in a power amplifier. Implementation using discrete elements resulted in an improvement of 8 dB in the C/I ratio of a power amplifier with two tones at the output of 34 dBm each. The final example illustrated gain suppression in a limiting amplifier, and demonstrated the rejection of the smaller of two signals in an amplifier driven into saturation.

Acknowledgment

The author wishes to acknowledge the support and encouragement of his doctoral adviser Prof. F. Rosenbaum, under whom much of this work was performed. D. Green and S. Kawano were also instrumental in developing nonlinear modeling techniques at the Microwave Laboratory of Washington University and contributed much to the present work. Thanks are also due to the author's previous employer, Central Microwave Co., and especially to R. Kiehne, for their assistance in the experimental evaluation of the components.

References

[1] M. S. Nakhla and J. Vlach, "A piecewise harmonic balance technique for determination of periodic response of nonlinear systems," *IEEE Trans. Circuits Syst.*, vol. CAS-23, Feb. 1976.

[2] V. Rizzoli, A. Lipparini, and E. Marazzi, "A general purpose program for nonlinear microwave circuit design," *IEEE Trans. Microwave Theory Tech.*, vol. MTT-31, pp. 762–770, Sept. 1983.

[3] D. R. Green and F. J. Rosenbaum, "Performance limits on GaAs FET large- and small-signal circuits," Washington Univ., St. Louis, MO, Rep. N00014-80-0318, Oct. 1981.

[4] SUPERCOMPACT, Communications Consulting Corp, Paterson, NJ.

[5] R. G. Hicks and P. J. Khan, "Numerical analysis of nonlinear solid-state device excitation in microwave circuits," *IEEE Trans. Microwave Theory Tech.*, vol. MTT-30, pp. 251–259, Mar. 1982.

[6] C. Camacho-Penalosa, "Numerical steady-state analysis of nonlinear microwave circuits with periodic excitation," *IEEE Trans. Microwave Theory Tech.*, vol. MTT-31, pp. 724–730, Sept. 1983.

[7] A. V. Oppenheim and R. W. Schafer, *Digital Signal Processing*. Englewood Cliffs, NJ: Prentice-Hall, 1975.

[8] R. J. Gilmore and F. J. Rosenbaum, "Modelling of nonlinear distortion in GaAs MESFETs," in *IEEE 1984 Int. Microwave Symp. Dig.*, June 1984, pp. 430–431.

[9] S. Kawano and F. J. Rosenbaum, "Modelling of third-order intermodulation distortion in GaAs MESFETs," M.S.E.E. thesis, Washington Univ., St. Louis, MO, Aug. 1983.

[10] A. Ushida and L. O Chua, "Frequency domain analysis of nonlinear circuits driven by multi-tone signals," *IEEE Trans. Circuits Syst.*, vol. CAS-31, pp. 766–779, Sept. 1984.

[11] Y. Takayama and K. Honjo, "Nonlinearity and intermodulation distortion in microwave power GaAs FET amplifiers." *NEC Res. Develop.*, no. 55, pp. 29–36, Oct. 1979.

[12] G. L. Heiter, "Characterization of nonlinearities in microwave devices and systems," *IEEE Trans. Microwave Theory Tech.*, vol. MTT-21, pp. 797–805, Dec. 1973.

[13] R. S. Tucker, "Third-order intermodulation distortion and gain compression in GaAs FETs," *IEEE Trans. Microwave Theory Tech.*, vol. MTT-27, pp. 400–408, May 1979.

[14] R. A. Minasian, "Intermodulation distortion analysis of MESFET amplifiers using the Volterra series representation." *IEEE Trans. Microwave Theory Tech.*, vol. MTT-28, pp. 1–8, Jan. 1980.

[15] A. Madjar and F. J. Rosenbaum, "A large-signal model for the GaAs MESFET," *IEEE Trans. Microwave Theory Tech.*, vol. MTT-29, pp. 781–788, Aug. 1981.

[16] C. Rauscher, "Frequency doublers with GaAs FETs," in *IEEE 1982 Int. Microwave Symp. Dig.*, pp. 280–282.

[17] R. Stancliff, "Balanced dual-gate GaAs FET frequency doublers," in *IEEE 1981 Int. Microwave Symp. Dig.*, pp. 143–145.

[18] E. Camargo *et al.*, "Sources of nonlinearity in GaAs MESFET frequency multipliers," in *IEEE 1983 Int. Microwave Symp. Dig.*, pp. 343–345.
[19] R. J. Gilmore, "Octave-bandwidth microwave FET doubler," *Electron. Lett.*, vol. 21, no. 12, pp. 532–533, June 6, 1985.
[20] R. J. Gilmore and F. J. Rosenbaum, "Circuit design to reduce third order intermodulation distortion in FET amplifiers," in *IEEE 1985 Int. Microwave Symp. Dig.*, pp. 413–416.
[21] F. E. Emery, "Solid-state limiting amplifiers," *Watkins-Johnson Co. Tech Notes*, vol. 5, no. 5, Sept./Oct. 1978.
[22] J. J. Jones, "Hard-limiting of two signals in random noise," *IEEE Trans. Inform. Theory*, vol. IT-9, pp. 332–340, Jan. 1963.
[23] J. A. Roberts, E. T. Tsui, and D. C. Watson, "Signal to noise ratio evaluations for nonlinear amplifiers," *IEEE Trans. Commun.*, vol. COM-27, pp. 197–201, Jan. 1979.

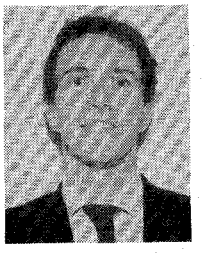

Rowan Gilmore (S'82–M'84) graduated from the University of Queensland, Australia, (with first class honors) in electrical engineering in 1976.

He worked as a communications engineer for the Overseas Telecommunications Commission (Aust.) until 1978, when he joined Schlumberger as a field engineer based in the Far East. In 1981, he joined the Microwave Laboratory at Washington University in St. Louis, graduating with an M.S.E.E. degree in 1982, and a D.Sc. degree in electrical engineering in 1984. From 1982 to 1985, he was employed as a senior design engineer at Central Microwave Co., St. Louis, MO. He is currently employed by Schlumberger Well Services, where he is project manager of their EPT (electromagnetic propagation tool). His interests are FET devices and circuits and computer-aided design.